LAWRENCE
LIVERMORE
NATIONAL
LABORATORY

LLNL-JRNL-827762

Quantitative XPS of plutonium: Evaluation of the Pu4f peak shape, Relative Sensitivity Factors and estimated detection limits

P. Roussel, A. J. Nelson

October 11, 2021

Surface and Interface Analysis

Disclaimer

This document was prepared as an account of work sponsored by an agency of the United States government. Neither the United States government nor Lawrence Livermore National Security, LLC, nor any of their employees makes any warranty, expressed or implied, or assumes any legal liability or responsibility for the accuracy, completeness, or usefulness of any information, apparatus, product, or process disclosed, or represents that its use would not infringe privately owned rights. Reference herein to any specific commercial product, process, or service by trade name, trademark, manufacturer, or otherwise does not necessarily constitute or imply its endorsement, recommendation, or favoring by the United States government or Lawrence Livermore National Security, LLC. The views and opinions of authors expressed herein do not necessarily state or reflect those of the United States government or Lawrence Livermore National Security, LLC, and shall not be used for advertising or product endorsement purposes.

Quantitative XPS of plutonium: Evaluation of the Pu4f peak shape, Relative Sensitivity Factors and estimated detection limits

Paul Roussel[1], Art J. Nelson[2]

1) AWE plc, Aldermaston, Reading, Berkshire, U.K. RG7 4PR

2) Lawrence Livermore National Laboratory, Livermore, CA 94551, United States

paul.roussel@awe.co.uk

Abstract

X-ray Photoelectron Spectra have been acquired from sputter cleaned α-plutonium and face centred cubic δ-plutonium-gallium 2 atomic % alloy and following the in-situ oxidation in the ultra-high vacuum of the analysis chamber. The differences in the Pu4f peak shape in these materials have been elucidated. Curve fitting parameters for various plutonium transitions are presented and Relative Sensitivity Factors have been determined. Examples of quantification of the plutonium spectra are provided and minimum detection limits are calculated for common impurities in/on plutonium metal.

UK Ministry of Defence© Crown owned Copyright 2021/AWE

Keywords:

Plutonium, X-ray Photoelectron Spectroscopy, Quantification, Detection limits

Introduction

Plutonium occurs at a unique position in the actinide series which is best represented by a comparison of metallic radii to the transition metals, lanthanides and actinides [1]. Here, the metallic radii decrease with increasing 5f electron population from thorium to neptunium similar to that observed with increasing d electrons in the transition metals indicative of involvement in bonding. From americium onwards the metallic radii follow a slight linear contraction similar to that found in the lanthanides where the 4f electrons are considered core-like and non-interacting. Between neptunium and americium is plutonium where the metallic radius has started to increase slightly when compared to neptunium. Furthermore, the metallic radii of the least dense allotropic phase of plutonium which is face centred cubic, lies roughly between that of neptunium and americium such that plutonium occupies a position in the periodic table where the 5f electrons are transitioning from itinerant to localized. Indeed, plutonium exhibits some unusual properties such as six temperature induced allotropic phases and a low melting point at 640 °C relative to transition metals and actinides. The room temperature phase, designated α-Pu, is monoclinic with a theoretical density of 19.86 gcm^{-3} [2]. The least dense phase at 15.92 gcm^{-3} is the δ-Pu or fcc structure which is stable between 320 and 460 °C which displays negative thermal expansion behaviour. The δ-Pu phase can be stabilized at room temperature by alloying with small quantities of either aluminium, americium, cerium, gallium, indium or zinc [2]. To understand the role of the 5f electrons in experimental data of α-Pu and a binary alloy of δ-Pu are often compared. Plutonium is also extremely reactive metal forming compounds, or alloys with the majority of the elements in the periodic table [2]. The oxophillic nature of plutonium means the metal is typically covered with an oxide film where the rate of reaction can progress at $cmhr^{-1}$ into the metal at room temperature [3]. In addition to the physical properties described above plutonium is radioactive and toxic which requires special handling facilities and scientific equipment modified or designed to contain possible contamination.

The ultra high vacuum (UHV) chambers of modern X-ray Photoelectron Spectrometers (XPS) provide a suitable containment vessel for small quantities of this hazardous material albeit with some form of additional modification, for example filtration of the vacuum exhaust. XPS measurements of the oxides of the trans-uranium elements were first reported by Veal *et al*. in 1977 [4]. This was followed by several reports of XPS measurements on α-Pu metal [5, 6]. The

ideal goal is to undertake routine quantitative XPS analysis on plutonium and plutonium containing materials as is carried out at most other laboratories on non-radioactive elements and materials. Quantitative XPS requires the use of Relative Sensitivity Factors (RSF) and to date five different RSF have been reported for the $Pu4f_{7/2}$ peak which range from 6.4 to 16.6 [7, 8, 9, 10, 11] relative to F1s value of 1.0. The RSF have been determined from either extrapolation of existing empirical RSF or manufacturers values [12] using the cross sections reported by Scofield [13] or experimentally determined from compounds. Interestingly, the largest and smallest reported RSF values are for same make and model of spectrometer. The incorrect choice of the RSF would lead to some significant errors in the quantification. In addition to the complications of quantification of Pu XPS using RSF, there are currently multiple interpretations of the $Pu4f_{7/2}$ peak shape of plutonium metal and alloys where the main peak is often accompanied by a lower intensity satellite to approximately 2.5 eV in binding energy [2]. This satellite feature complicates the determination of the accurate peak area to be used for quantification and further investigations into its origin are required.

We report here XP spectra acquired from α-Pu and δ-Pu(Ga) 2 atomic % alloy obtained using identical parameters. From the analysis of the X-ray induced Auger data, the Pu4f peak shape and intensity we show that the satellite feature at 2.5 eV higher binding energy most likely occurs from Pu^{3+} impurities and the main difference between the two samples is a slightly narrower Full Width Half Maximum (FWHM) in the α-Pu sample. RSF have been determined for the $Pu4p_{3/2}$, $Pu4d_{5/2}$, Pu4f and $Pu6p_{3/2}$ transitions and applied to quantification of the plutonium-oxygen stoichiometry during initial stage of oxidation and the alloy Ga concentration. Finally, minimum detection limits for common impurity elements are calculated.

Experimental

XPS spectra were acquired with a Physical Electronics Quantera II using 200 μm spot size monochromatic Al *K*α X-rays with the electron analyser operating in the "scanned mode" with a base pressure of $5x10^{-9}$ torr. All spectra were acquired with the sample angle of emission of 45º. The spectrum acquisition parameters are detailed in Table 1. A sample of electro refined α-Pu, δ-

$Pu_{0.98}Ga_{0.02}$ alloy and an epitaxial GaN single crystal were mounted on the same platen for analysis. Sample cleaning was performed by in-situ argon iom sputtering using the 4 keV, 2 x 2 mm raster size, 4.2 μA setting. The binding energy scale was calibrated according to the manufacturer's procedure and in agreement with ISO 15472 "Calibration of energy scales". Three further spectra are presented in the Figures for comparison that were acquired using different spectrometers as detailed now. The Ga (LMM) X-ray induced Auger spectrum of sputter cleaned gallium were acquired using a Physical Electronics Versaprobe II spectrometer using a 100 μm spot size monochromatic Al *K*α X-rays, a pass energy of 23.5 eV and a step size of 0.1 eV. Pu4d and 5d spectra of a Pu_2O_3 film on metal substrate were acquired using VG Escalab II spectrometer employing non-monochromatic Mg *K*α X-rays, a pass energy of 20 eV and a step size of 0.1 eV.

Table 1. Spectrum acquisition parameters

Region	**Binding energy range (eV)**	**Step size (eV)**	**Pass energy**
Survey	0 - 1300	0.5	280
$Pu4p_{3/2}$ / Ga2p	1105 - 1145	0.1	55
$Pu4d_{5/2}$	780 - 820	0.1	26
O1s	523 - 543	0.1	26
Pu4f	420 - 450	0.1	26
C1s	278 – 298	0.1	26
Pu5d / Ga3p	90 - 125	0.1	26
Valence / $Pu6p_{3/2}$ / Ga3d	-5 - 30	0.1	55

Initial data inspection and Linear Least Squares (LLS) analysis was undertaken using Physical Electronics Multipak version 9.8. Peak fitting was performed using CASA XPS version 2.3.24 [14]. A Shirley background was fit to the Pu spectra and linear background was used for the O1s region with the end point average set to ten. Voigt (LA) and asymmetric Voigt with tail dampening (LF) peak shapes were employed in the fitting process as outlined in a recent guide on

asymmetric line fitting [15]. The line shape was optimised using the 'Test Peak Model' function and position and parameters were determined on the reference or pure material spectra where possible. Once the peak model was optimised the position or spin orbit splitting, Full Width Half Maximum (FWHM) were fixed and in the case where the region consisted of two peaks e.g. spin-orbit splitting the intensity ratio of the two peaks was constrained and propagated to the other spectra. The peak fitting parameters are detailed in Table 2 as recommended in ISO 19830 "Minimum reporting requirements for peak fitting in X-ray Photoelectron Spectroscopy". After the area was determined from software the data was further corrected in Excel for the asymmetry parameter [16] and Transmission Function Correction (TFC) as described in the Multipak software manual. RSF for oxygen and gallium were taken from Multipak software manual. The area of the O2s was constrained to 0.378 of the $Pu6p_{3/2}$ peak in Pu^{3+} oxide and the intensity of the peak attributable the $Pu6p_{3/2}$ in α-Pu at 18.8 eV was constrained to 0.576 of the lower binding energy peak at 16 eV. Electron Attenuation Lengths, EAL, were calculated following the method reported by Seah [17] using the band gap value of 0.7 eV reported for Pu_2O_3 [18]. Estimated detection limits were calculated following the procedure outlined in ISO 19668 using the survey spectrum shown in Figure 1, a coverage factor of 2.33, with the background noise calculated as the standard deviation of counts, RSF values used were taken from the Multipak software manual or determined here corrected for TFC, asymmetry parameter with the Pu4f spin orbit doublet as the reference peak.

Table 2. Peak fitting parameters used for the quantification of plutonium, oxygen and gallium with estimated uncertainty of the position and FWHM in parenthesis calculated following the methodology in ISO 19830. Note the fitting parameters for the pure Pu5d peaks could not be determined due to the unusual line shape and have not been included in the table below (see text for discussion)

	Background range (eV)	Line shape	Position (eV)	FWHM (eV)
Pu^{3+} oxide $Pu4p_{3/2}$	1106 - 1144	LF(0.3, 0.9, 25, 140)	1123.3 (0.024)	6.8 (0.037)

Pu^0 $Pu4p_{3/2}$	1106 – 1144	LF(0.3, 0.9, 25, 140)	1120.9 (0.09)	7.6 (0.14)
Pu^{3+} $Pu4d_{5/2}$	781 - 819	LF(0.54, 0.86, 25, 140)	799.9 (0.018)	6.1 (0.034)
Pu^0 $Pu4d_{5/2}$	781 - 819	LF(0.3, 0.9, 25, 140)	797.7 (0.012)	6.2 (0.021)
Pu^{3+} oxide $Pu4f_{5/2}$	420 – 448	LF(0.43, 0.75, 50, 233)	438.1 (0.005)	2.5 (0.009)
δ-$Pu4f_{5/2}$ metal	420 – 448	LF(0.28, 0.9, 164. 240)	435.1 (0.002)	1.2 (0.004)
α-$Pu4f_{5/2}$ metal	420 – 448	LF(0.28, 0.9, 164. 240)	435.0 (0.001)	1.14 (0.002)
Pu^{3+} oxide $Pu4f_{7/2}$	420 – 448	LF(0.43, 0.75, 50, 233)	425.3 (0.004)	2.03 (0.007)
δ-$Pu4f_{7/2}$ metal	420 – 448	LF(0.28, 0.9, 164. 240)	422.2 (0.001)	1.07 (0.006)
α-$Pu4f_{7/2}$ metal	420 – 448	LF(0.28, 0.9, 164. 240)	422.2 (0.001)	0.97 (0.002)
Pu^{3+} $Pu6p_{3/2}$ O2s (0.378%)	12 – 27	LA(1, 643) LA(1, 643)	17.8 (0.004) 22.1 (0.0018)	3.2 (0.009) 4.4 (0.004)
$Pu6p_{3/2}$ metal	10 - 25	LA(1, 643) LA(1, 643)	16 (0.03) 18.8 (0.03)	3.1 (0.08) 3.1 (0.06)
O1s oxide	526 -536	LA(1.53, 243)	530.6 (0.006)	1.1 (0.01)
O1s hydroxyl	526 - 536	LA(1.53, 243)	532.7 (0.03)	1.98 (0.1)
$Ga2p_{3/2}$ $Ga2p_{1/2}$	1106 – 1144	LA(1.53, 243)	1114.7 (0.0008) 1141.5 (0.001)	1.8 (0.002) 1.8 (0.003)
Ga3d	10 - 25	LA(1, 643)	17.4 (0.002)	1.6 (0.004)

Results and discussion

The survey spectrum for sputter cleaned α-Pu is shown in Figure 1 with the major photoemission lines highlighted. From Figure 1 there are a range of possible plutonium core level peaks that could be used for quantification with the most intense peaks attributable to the Pu4f spin-orbit doublet. In addition to the photoemission line from plutonium a small residual O1s signal is also

detectable which is typical for this highly reactive metal. Note, that the C1s binding energy coincides with the broad low intensity $Pu5p_{1/2}$ peak. The expanded, higher resolution Pu4f spectrum for α-Pu is shown at the top of Figure 2 and consists of the spin orbit doublet of asymmetric peaks with lower intensity shoulders or satellites approximately 2.5 eV to higher binding energy. Prior to determining the experimental RSF for the Pu4f spin orbit doublet it would be useful to understand the origin of these satellite peaks to confirm if they contribute to the intensity of α-Pu spectrum. There are currently three different interpretations of this peak structure in plutonium metal and alloys, the first is that consists of three peaks from the $5f^4$, $5f^5$ and $5f^6$ final state multiplet structure as calculated from Anderson impurity model with different fractional percentages depending on the crystallographic phase of plutonium [19]. While final state multiplets are expected in XPS of metals or materials with unpaired valence electrons that display *LS* or Russell-Saunders coupling [20], high energy electron energy loss spectroscopic measurements have shown this does not apply to plutonium [21]. Furthermore, the expected increase in spin orbit splitting between different spin states has not been observed in plutonium [22]. The second interpretation is based on the screening model reported by Fuggle *et al*. [23] whereby the unoccupied states are pulled below the Fermi level, E_F, on creation of core hole in the XPS experiment and the asymmetric line shape is the 'well screened' peak and the satellite feature occurs from 'poor screening'. This model has shown to be an excellent description for the 3d XPS in the lanthanides, the 4f spectrum of thorium metal [23] and americium [24] and therefore should afford a good interpretation of the Pu4f spectrum of the plutonium metal phases. The height of the poorly screened peak is often used as an indication of the degree of localization in the material and for plutonium materials the satellite feature typically has an increased intensity relative to the asymmetric peak for δ-Pu(Ga) alloys when compared to Pu4f spectrum of α-Pu [25, 26, 27]. Interestingly, inverse photoemission measurements (IPES) of the unoccupied states show little difference between α-Pu and δ-Pu(Ga) phases [28] and therefore only a small or negligible difference would be expected between the well and poor screened peaks of the Pu4f spectrum.

The third interpretation is that the satellite peak occurs from localization occurring from impurities that form Pu^{3+} either on the surface or dissolved in the bulk material as the binding energy position and line shape are similar to that reported for PuC [29], Pu_2O_3 [30], PuN [31], PuH_x (x = 2-3) [32]. An example of the localized or Pu^{3+} Pu4f spectrum from Pu_2O_3 acquired

from the native oxide film on the α-Pu sample is included in Figure 2 for comparison. Furthermore, previously reported angle dependant XPS acquired on both α-Pu and δ-Pu(Ga) alloy samples at multiple laboratories all show that the satellite intensity increases with electron emission angle and this peak is related to the surface species [18, 25, 26, 33, 34]. In addition to the information described above, one of the most significant arguments for impurities comes from the irreproducibility of the Pu4f peak shape acquired from sputter cleaned α-Pu and δ-Pu(Ga) alloys on different samples, or using different spectrometers or at different laboratories. For comparison, the XPS spectra reported for thorium and the lanthanides are highly reproducible regardless of sample, spectrometer or laboratory. A further consideration for data acquired on δ-Pu(Ga) alloys using Al *K*α radiation is that the binding energy of the Pu4f coincides with the X-ray induced Auger Ga(LMM) peaks and a spectrum of sputter cleaned Ga metal has been included in Figure 2. From the discussion above it is clear that any data analysis will require careful consideration to determine what effects the Pu4f peak shape.

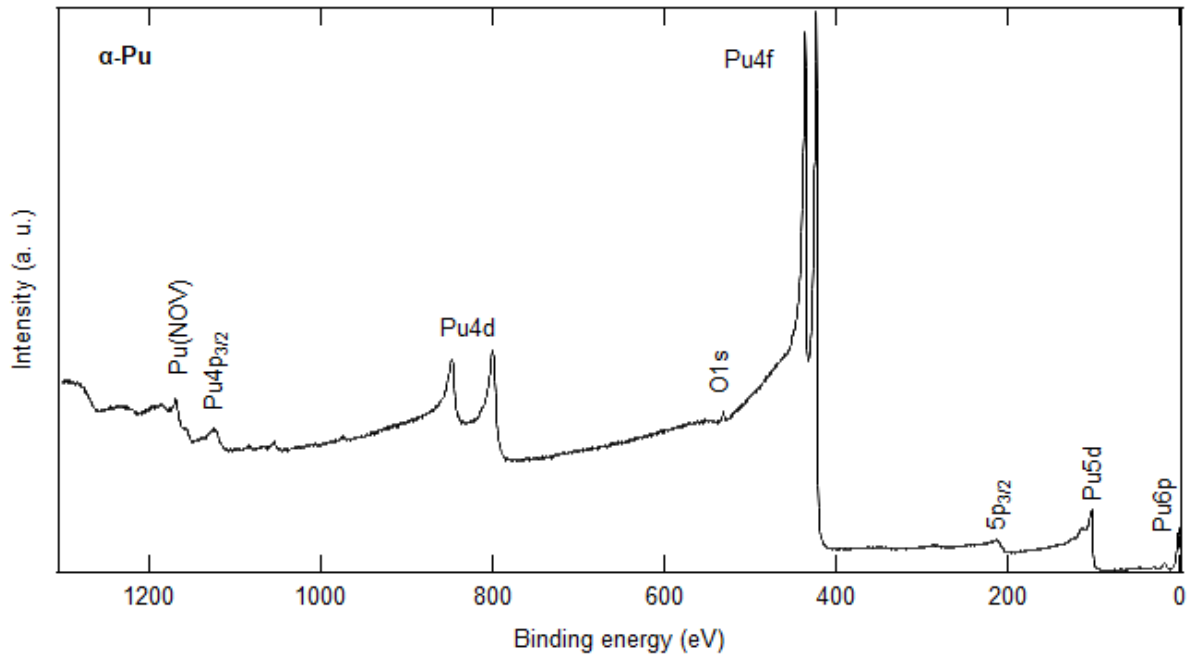

Figure 1. XPS survey spectrum of sputter cleaned α-Pu with the prominent photoemission lines labelled.

As well as the α-Pu sample described above, a sample of δ-Pu(Ga) alloy was mounted on the same platen and the sputter cleaned Pu4f spectrum is shown in Figure 2. From Figure 2 it is

clear that the satellite peaks are lower in intensity relative to the asymmetric peak in the δ-Pu(Ga) sample compared to the α-Pu sample measured here. The Pu4f spectrum of δ-Pu(Ga) shown in Figure 2 compares favourably to previously reported spectra for α-Pu [18, 27]. Subtraction of the normalized Pu4f spectra of δ-Pu(Ga) from α-Pu shown in Figure 2 afforded a difference spectrum where the positive deviation agrees with the Pu_2O_3 spectrum suggesting the satellite feature is attributable to oxide or Pu^{3+} impurities that afford an similar peak position and shape (see supporting information for the difference spectrum). Interestingly, a negative deviation or missing intensity is observed on the high binding energy side of the asymmetric peaks in the difference spectrum of δ-Pu(Ga) that most likely occurs from a slightly broader FWHM in the alloy sample. Curve fitting parameters were developed for the Pu4f spin orbit doublet for both α-Pu and δ-Pu(Ga), first by obtaining a line shape from the Pu_2O_3 spectrum shown in Figure 2 and then fitting asymmetric peaks for the metal spin orbit doublet and applying constraints as described in the experimental section. The asymmetric line shape is typical for actinide metals [35] and was found to have a FWHM 0.1 eV greater in the δ-Pu(Ga) spectrum compared to the α-Pu sample. As the spectra were acquired under identical conditions the increased FWHM is indicative of a shorter core hole lifetime reflective of the different chemical environment in the δ-Pu(Ga) alloy [36]. Curve fitting the Pu4f spectra shown in Figure 2 afforded satellite peak areas of approximately 19.2 and 9.6 % relative to the asymmetric spin orbit doublet for α-Pu and δ-Pu(Ga) respectively.

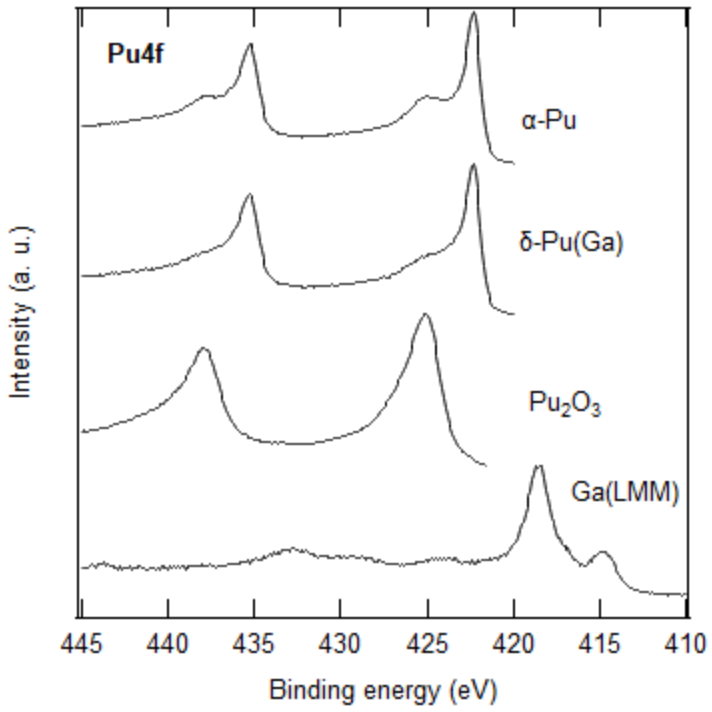

Figure 2. Pu4f XPS spectra of α-Pu (top), δ-Pu(Ga), Pu_2O_3 and the X-ray induced Auger spectrum of Ga(LMM) (bottom) in the same energy region.

The width and intensity of the X-ray induced Auger peaks can afford information on the amount of screening and localization in a material [37]. The survey spectra covering the Pu(N_7O_5V) X-ray induced Auger energy range are identical for both α-Pu and δ-Pu(Ga) at the resolution acquired here (see Supporting Information). Therefore, regardless of the amount of possible localization or screening this result suggests the relative intensity of the well and poorly screened peaks in the Pu4f spectra will be the same or very similar for both α-Pu and δ-Pu(Ga) which is in agreement with the IPES measurements [28]. Combining the kinetic energy of the Pu(N_7O_5V) and $Pu4f_{7/2}$ afford an identical modified Auger parameter of 743.3 eV for both α-Pu and δ-Pu(Ga) as has been reported by Larson and Motyl [38].

Ideally the experimental RSF should be determined from the intensity of the photoionisation peak from a pure, flat plutonium sample and compared to a known reference sample acquired using the same spectrometer. As the Pu4f intensity of the pure metal could not be acquired and an attempt to estimate the value using a similar method described in a recent practical guide on quantitative XPS by Shard [39]. To achieve this the in-situ oxidation of the

sputter cleaned α-Pu sample was followed sequentially acquiring Pu4f and O1s spectra for approximately four hours. This experiment was also repeated on the δ-Pu(Ga) sample for comparison. Both experiments showed similar behaviour, that with time the localized Pu4f peak shape for Pu^{3+} oxide increased in intensity at the expense of the metal Pu^{0} asymmetric line shape with the concomitant increase in the O1s intensity (see supporting information). In addition, the binding energy of Pu4f spin orbit doublet of Pu^{3+} oxide decreased by 0.6 eV with increasing concentration finishing with a $Pu4f_{7/2}$ peak position of 424.8 eV in agreement with previously reported values [5, 10, 30, 34]. Initially the O1s spectrum displayed a single peak positioned at 530.6 eV typical for plutonium oxide [10] and with time an additional peak at 532.7 eV grew in, albeit at significantly lower intensity. This latter peak has been attributed to either formation of surface hydroxyl or the possible absorption of carbon monoxide [9]. These two experiments had several interesting observations. The first showed there is a linear correlation of the localized Pu^{3+} Pu4f peak shape and the O1s intensities with time in both experiments adding confidence to the interpretation offered here, that the satellite feature is from impurities. The second observation showed the estimated Pu4f intensity obtained from extrapolation of a plot of Pu^{0} vs Pu^{3+} areas (Figure 3) was lower for the δ-Pu(Ga) sample compared to α-Pu material even after correction for the EAL. Presumably this occurs from lower density and therefore decreased Pu atom concentration in the fcc stabilized alloy. Indeed, comparison of the EAL (Electron Attenuation Length) corrected intensity ratio of α-Pu / δ-Pu(Ga) is within < 3 % to the theoretical Pu atom density ratio [40]. However, when the Pu4f intensity of the metal and alloy includes the Pu^{3+} contribution as in either the poor screening model then the comparison to the theoretical atom density is inferior at ≈7 %, again, supporting the interpretation that the Pu4f satellites in the spectra of α-Pu and δ-Pu(Ga) alloys predominantly occur from Pu^{3+} impurities. Therefore, the following work presented here will treat the asymmetric peak as occurring from Pu^{0} representative of the metal or alloy and the satellite peak occurring from Pu^{3+} oxide impurities here, but we note that this could either be any impurity element that reacts with plutonium to form this peak position and shape which, as previously highlighted includes H, C, N, O but is not exclusively restricted to these elements, for example, both PuSb [41] and $PuFe_2$ [42] also show a very similar profile and energy.

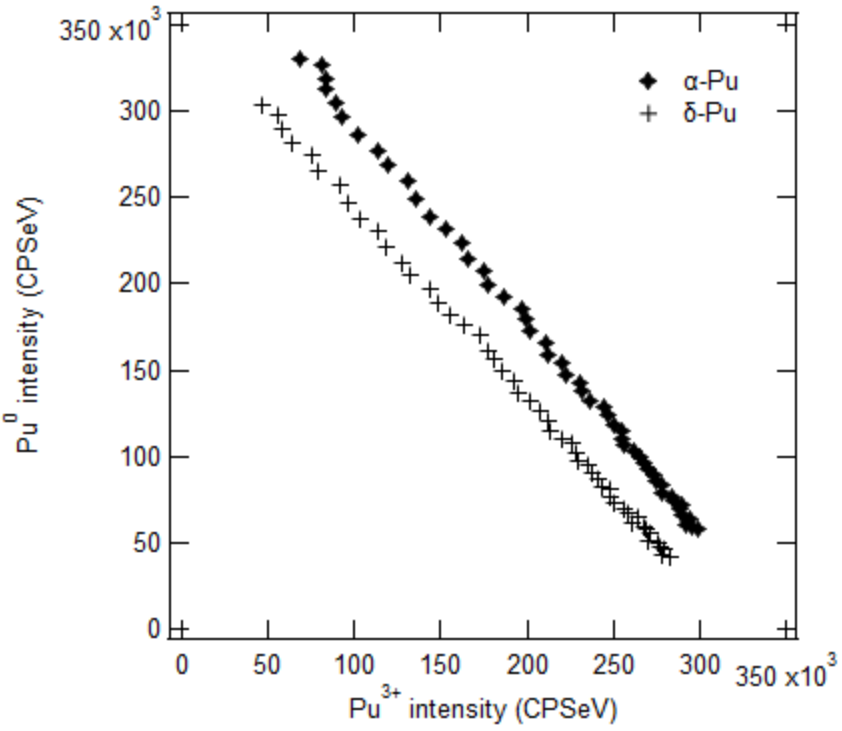

Figure 3. The intensity of Pu^0 vs Pu^{3+} of the Pu4f data following the in-situ oxidation of α-Pu and δ-Pu(Ga) in UHV used to extrapolate to obtain an estimated intensity for Pu^0 in both phases.

Here we have ignored the possible effect of the Ga(LMM) X-ray induced Auger peak (Figure 2). Although none of the main peaks of the Ga(LMM) directly overlap with the position of the Pu4f spin orbit doublet there is a broad, low intensity signal between the $Pu4f_{7/2}$ and $Pu4f_{5/2}$. Therefore, at the low Ga concentration in the material studied here it is likely that there will only be a very small contribution to the background intensity of the Pu4f peak shape. However, to better understand the Ga(LMM) contribution to the Pu4f spectrum and the line broadening discussed earlier, alloys containing larger quantities of Ga should be studied but this is outside the scope of this work.

Having now established an intensity for the Pu4f spin orbit doublet it is possible to determine the RSF. The experimental elemental Pu4f RSF was calculated from the extrapolated estimated intensity of α-Pu discussed above and compared to the $Ga2p_{3/2}$, Ga3p and Ga3d regions of a GaN reference sample mounted on the same sample platen. The experimental intensities were corrected for Transmission Function Correction (TFC), spectrometer operating geometry and respective Ga RSF as described in the Experimental section. This afforded an experimental RSF

for the Pu4f region of 20.41 which is slightly lower than the value reported by García Flores and Pugmire of 20.62 relative to F1s value of 1.0 [9] and slightly higher than the extrapolated values [8]. The value for the Pu4f region was then used to calculate the RSF for the $Pu4p_{3/2}$ (Figure 4), $Pu4d_{5/2}$ (Figure 5) and $Pu6p_{3/2}$ (Figure 6) and these are listed in Table 3. Included in Figures 4 to 6 are the spectra for α-Pu, δ-Pu(Ga), Pu_2O_3 and where the peaks overlap the respective spectrum from the Ga reference sample. A similar curve fitting methodology used for the Pu4f region to determine the areas of the Pu metal and Pu^{3+} impurity peak position, shape and FWHM was applied to the other plutonium transitions. There are several key observations from the other Pu transitions. These include that the Pu^{3+} oxide peak does not form a discrete shoulder or satellite peak either the $Pu5d_{5/2}$ or $Pu4p_{3/2}$ spectra, presumably due to the larger FWHM compared to the Pu4f region. It is likely the increased FWHM of the $Pu4d_{5/2}$ and $Pu4p_{3/2}$ will mask any difference between the α-Pu and δ-Pu(Ga) phases reported earlier in the Pu4f peak shape. The $Pu6p_{3/2}$ transition for Pu^{3+} oxide affords a single peak at 17.8 eV that overlaps with the O2s transition at 22.1 eV and the position, FWHM and intensity ratio of these two peaks were constrained when determining the line shape parameters from α-Pu spectrum (Table 2 and Figure 6). The spectrum of α-Pu (Figure 6) shows the broad low intensity feature between 13 and 21 eV attributable to $Pu6p_{3/2}$ likely consists of two peaks at 15.5 and 17.8 eV with the latter more intense. A two peak structure for the $Pu6p_{3/2}$ has been previously reported to occur from hybridisation with the valence band from analogy to the high resolution XPS data acquired on a uranium single crystal [43]. However, we note that the peak at 17.8 eV can also be curve fit using the parameters for Pu^{3+} oxide detailed in Table 2 and while using a two peaks to represent the metal will afford better fitting statistics it could be physically meaningless [44]. The only other reported XPS spectrum for the $Pu6p_{3/2}$ peak using non-monochromatic Mg *K*α afforded a broad peak in the same energy range shown in Figure 6 [6]. Therefore, two approaches to curve fitting the $Pu6p_{3/2}$ peak in α-Pu were tested. First, the $Pu6p_{3/2}$ peak was fit using a single peak to represent the metal and the two constrained peaks representing the oxide as discussed earlier. This afforded an oxide quantity of approximately 53 % after correcting for Pu atom density. The second approach fit the $Pu6p_{3/2}$ peak of α-Pu using two peaks constrained to having equal FWHM, as well as the two peaks representing the oxide and this afforded an oxide quantity of 11.6 %. Both approaches suffered from having the $Pu6p_{3/2}$ oxide peak position constrained which may be incorrect as the in-situ oxidation experiments discussed above showed. Considering the EAL for the $Pu6p_{3/2}$ transition should be the most

representative of the bulk α-Pu sample and combined with the information described above suggest that the method using two peaks to be correct. Indeed, for oxide quantity found from using one peak we would expect significant changes to the valence band and the other Pu transitions as well as the presence of an O1s signal which was not observed. Finally, all the localized peaks from Pu^{3+} oxide all occur 1.5 – 2.5 eV to higher binding energy above the Pu^{0} or metal positions.

There are certain caveats to the use of the RSF values presented in Table 3. First the values are specific to the spectrometer and manufacturers software package used in this study, however, they should be applicable to other spectrometers operating in a similar geometry and with the TFC determined by the same methodology and to the best of the our knowledge this covers two thirds of the spectrometers currently available that have been used to analyse plutonium containing materials. Secondly, the values represent elemental RSF as defined in ISO 18118 "Guide to the use of experimentally determined relative sensitivity factors for the quantitative analysis of homogeneous materials" and further determination of the average matrix RSF could not be undertaken as the values as the elastic scattering parameters are only reported for Z up to 83 (Bi). However, the use of the RSF for quantitative XPS as detailed below is augmented with the asymmetry factor and TFC as defined in the software manual to afford the corrected RSF and where possible the EAL and atom density of the respective element. Finally, the use of RSF are recommended for homogenous materials only, which, for plutonium is possible in the oxides and as this work has shown extremely difficult for the metal or alloy due to oxide or impurities.

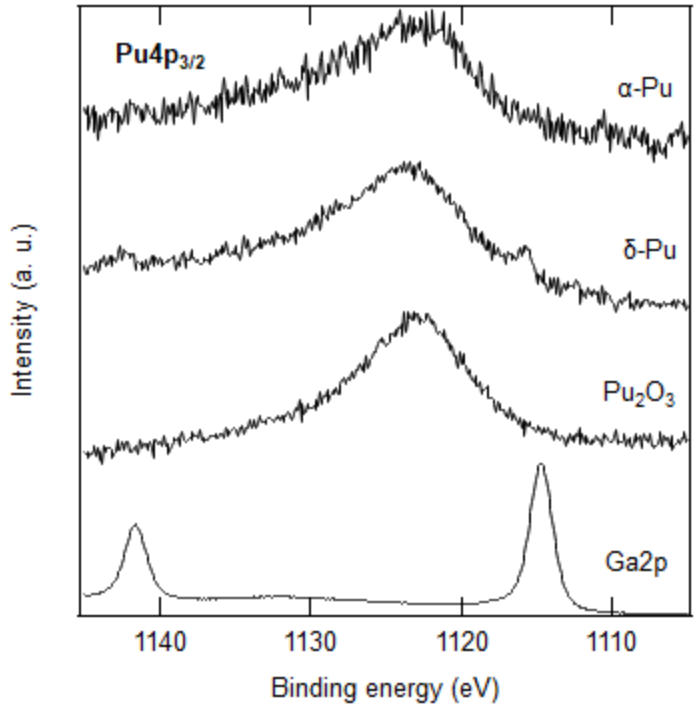

Figure 4. $Pu4p_{3/2}$ XPS of α-Pu, δ-Pu(Ga) Pu_2O_3 and the Ga2p spectra of GaN (top to bottom as labelled in the Figure)

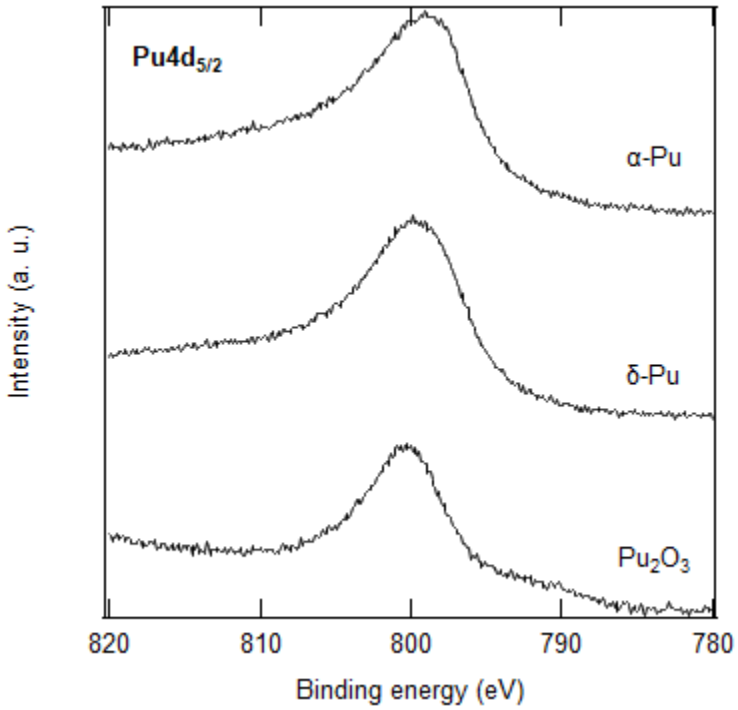

Figure 5. $Pu4d_{5/2}$ XPS of α-Pu and δ-Pu(Ga) and Pu_2O_3 (note the spectrum of Pu_2O_3 was acquired on a different spectrometer using no-monochromatic Mg Ka radiation)

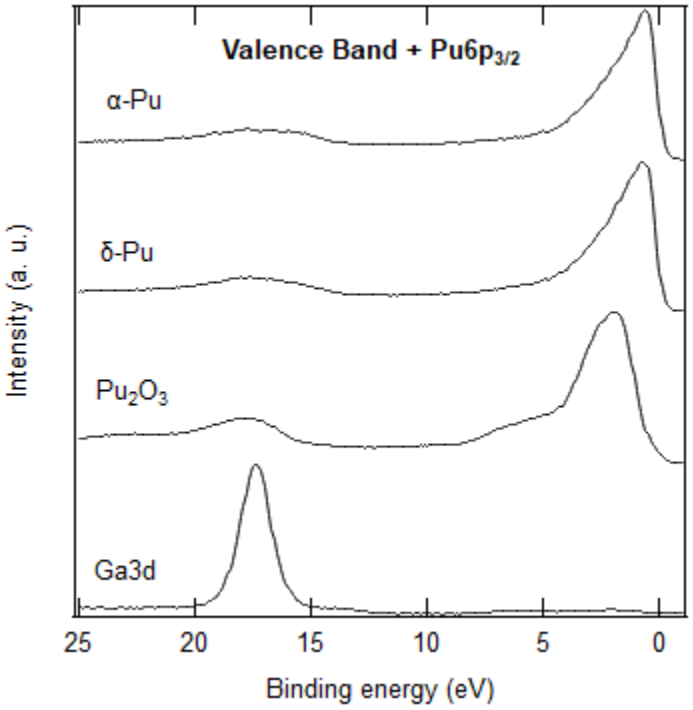

Figure 6. Valence band XPS including the $Pu6p_{3/2}$ transition between 15 and 20 eV for α-Pu, δ-Pu(Ga), Pu_2O_3 and the Ga3d acquired from sputter cleaned GaN (from top to bottom as indicated on the Figure)

Table 3. Experimental determined elemental RSF values for various Pu photoionization peak areas.

Transition	**RSF**
$Pu4p_{3/2}$	0.88
$Pu4d_{5/2}$	4.92
Pu4f ($4f_{7/2}$, $4f_{5/2}$)	20.42 (11.61, 8.8)
$Pu6p_{3/2}$	0.16

There is one notable omission from Table 3 and as shown in Figure 1 the Pu5d transition is relatively intense and it would be useful to determine an RSF value for these peaks. The Pu5d spectra for α-Pu, δ-Pu(Ga), Pu_2O_3 and the Ga3p are shown in Figure 7. The Pu5d spectrum for α-Pu consists of an asymmetric peak at 101.4 eV with a satellite to 1.5 eV to higher binding energy. Comparison to the spectrum of α-Pu to δ-Pu(Ga) shows this satellite intensity is reduced in the alloy sample relative to the asymmetric peak and was also found to decrease with sputtering time. The satellite peak position is identical to that of Pu_2O_3 spectrum albeit the one shown in Figure 5 was acquired on a different spectrometer using a non-monochromatic X-ray source. A similar Pu5d spectrum for Pu_2O_3 can be obtained by subtracting the Pu5d data of δ-Pu(Ga) from the α-Pu shown in Figure 7. In addition to the asymmetric peak at 101 eV in the spectra of α-Pu and δ-Pu(Ga), there is broad feature between 111 and 118 eV which decreases in intensity in the Pu_2O_3 spectrum. The Pu5d peak shape does not show a clear spin orbit doublet as found in thorium and uranium metal [45]. Hence, it was not possible to determine a physically realistic curve fit model and appropriate intensity that represents this transition for the metal to calculate a RSF.

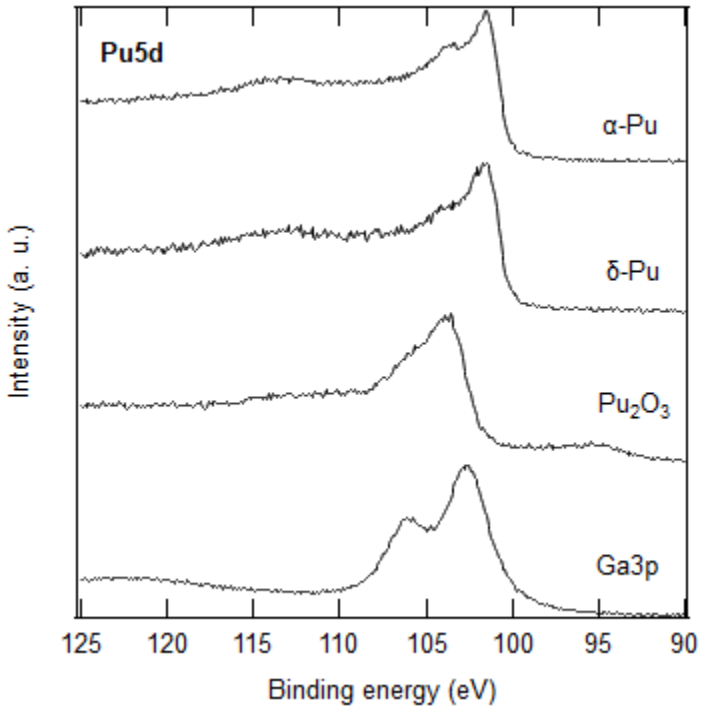

Figure 7. The Pu5d spectra of α-Pu, δ-Pu(Ga), Pu_2O_3 and the Ga3p of GaN. Note the Pu_2O_3 spectrum was acquired using a different spectrometer employing non-monochromatic Mg *K*α X-ray source and the peak to lower binding energy, 90 – 100 eV is from the satellites

Having now determined curve fit models and RSF values for multiple Pu transitions it would be useful to demonstrate the applicability in a range of examples. The advantage of having multiple transitions at different binding energies allows information to be determined from different depths (EAL). This is particularly useful if the spectrometer does not have the ability to alter the sample angle with respect to the electron analyser to change the angle of electron emission or range of angles is limited as in the work presented here due to the large sample platen used. Assuming the Pu^{3+} peak area is attributable to stoichiometric Pu_2O_3 and correcting the intensity for the Pu atom density the oxide contribution is 16.2, 10.4, 10.2, 11.6 % for the $Pu4p_{3/2}$ $Pu4d_{5/2}$, Pu4f and $Pu6p_{3/2}$ peaks and this corresponds to EAL values of 0.87, 1.33, 1.83 and 2.35 nm respectively. The higher oxide contribution with smallest EAL from the analysis of $Pu4p_{3/2}$ peak is indicative of surface contamination. Whereas the approximate value of 10-11 % oxide for the larger EAL suggest that it is a bulk or near surface impurity with respect to the surface. It is highly likely that some of the impurities exist from the sputtering process embedding or knocking on impurities into the sample and damaging the surface [46]. Finally, it should be stressed that the 10-11 % impurities exist in the surface / near-surface region with depth probed in the XPS measurement of 3 EAL i.e. < 7 nm in metal and alloy, do not reflect the bulk chemical analysis which show impurity content < 1 % by weight [2].

We now turn to investigating the Pu-O stoichiometry during the initial stage of oxidation in UHV using the data sets described earlier. The Pu^{3+} and O1s signal intensities were corrected for the TFC, RSF asymmetry parameter, and the EAL for the respective kinetic energy of each transition. The O1s:Pu^{3+} ratio is shown in Figure 8 for both the individual oxide O1s peak and the summed intensity from the oxide and hydroxyl shoulder. Both O:Pu ratios show a rapid increase during the initial oxidation followed by a constant value for the sum of the oxide and hydroxyl whereas the oxide stoichiometry decreases slightly with time. The difference between the two datasets represents the growth of the hydroxyl intensity. The O:Pu ratio of the oxide and hydroxyl affords an average stoichiometry of $PuO_{1.6}$ which is in the range reported for the cubic sesquioxide compound [47]. The O:Pu ratio for the oxide peak decreases from just above 1.25 to an average

stoichiometry of approximately $PuO_{1.15}$ in agreement with the characterization of sub-stoichiometric plutonium oxide reported by Garcia-Flores and Pugmire [9]. Applying the same data treatment to the in-situ oxidation of the δ-Pu(Ga) sample gave O:Pu ratios that are essentially identical to those shown in Figure 8 and this afforded confidence in the data analysis as it is expected that the oxide composition should not be influenced by the substrate material unless the alloying element has a significant role. Thermodynamic properties and previously reported XPS and AES data show that the plutonium is preferentially oxidised over the gallium [48].

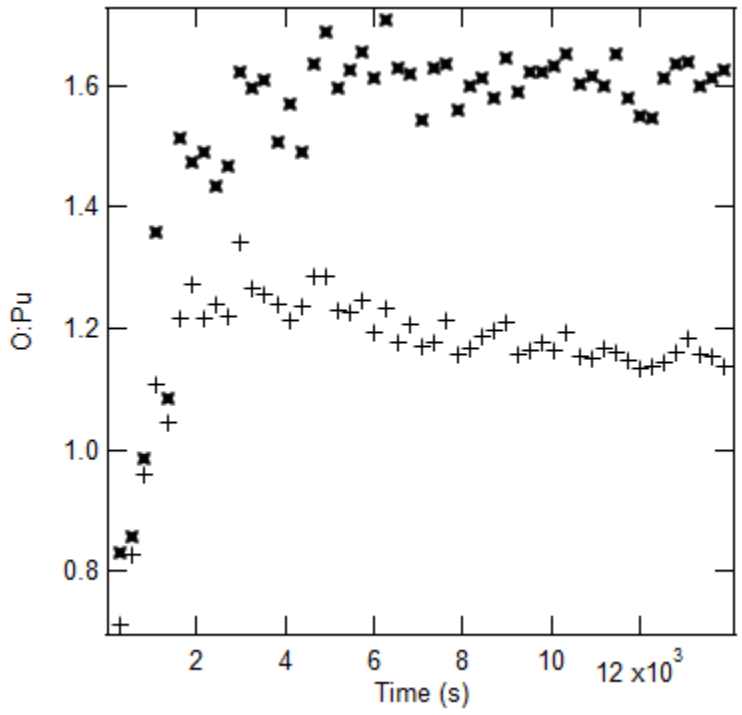

Figure 8. The O/Pu^{3+} ratio during the in-situ oxidation of α-Pu determined from the Pu4f and O1s intensity corrected for RSF, asymmetry parameters, TFC and EAL.

Finally, we address the problem of Ga quantification. As has been shown in Figures 2-7, the various Ga core level lines overlap with those of plutonium. Specifically these are the Ga2p overlaps with the $Pu4p_{3/2}$ (Figure 4), the Ga(LMM) X-ray induced Auger overlaps with the Pu4f (Figure 2), the Ga3p overlaps with the Pu5d (Figure 7) and the Ga3d overlaps with the $Pu6p_{3/2}$ peaks (Figure 6). Initial quantification was attempted using LLS method and the spectra presented in Figures 4 and 6 was unsuccessful affording Ga concentrations of 0.41 and 4.4 % for the Ga2p, $Pu4p_{3/2}$ and Ga3d, $Pu6p_{3/2}$ regions, respectively. The possible failure to obtain Ga concentrations

closer to the expected quantity might be as the Ga2p and 3d were acquired from a GaN sample. Next, curve fitting of the spectra for both Pu^0, Pu^{3+} and Ga peaks was attempted starting with the Ga2p, $Pu4p_{3/2}$ region. Interestingly, a similar example has been presented where the Ga2p spin orbit doublet exist on either side of the $La3p_{3/2}$ peak [39]. Applying the same curve fitting methodology described for the $La3p_{3/2}$ and Ga2p to quantify the plutonium alloy here afforded a Ga concentration of 1.3 % which is lower than the expected value. One possible reason for a concentration lower than expected is from the preferential sputter removal of gallium which has been previously reported for Pu(Ga) alloys [25] which will show he largest effect in due to the relatively small EAL of the Ga2p and $Pu4p_{3/2}$ transitions. Therefore, to minimise the effects of preferential sputtering the intensity of the $Pu6p_{3/2}$ and Ga3d peaks were evaluated which afforded the highest kinetic energy and thus the largest EAL or depth probed. Curve fitting for both Pu^{3+} and Pu^0 and the Ga3d afforded a Ga concentration of 1.96 %, almost identical to the expected quantity. While this has shown to be reasonably successful in this example it would be useful to test this methodology on different alloy concentrations to confirm the applicability.

The work presented so far supports the hypothesis that the satellite peaks in the Pu4f spectra of sputter cleaned plutonium and plutonium alloys occurs from surface impurities. However, we cannot discount the possibility that a very low intensity satellite due to poor screening exists at the same position as the Pu^{3+} impurities or is masked by this peak. Indeed, the poorly screened satellites in the spectrum from sputter cleaned thorium occurs at the same binding energy of ThO_2 [49] and an alternative explanation of the surface sensitivity of the satellite feature as shown in the angle dependant XPS studies could be explained by a surface core level shift as reported by Gerkin *et al*. for the lanthanide metals [50]. Clearly the Pu4f peaks will be the most sensitive to effects from impurities or possible screening and to fully help this interpretation it would be useful to understand the estimated detection limits of common contaminants. Shard has reported a methodology to calculate the estimated detection limits [51] which has been further developed into ISO 19668:2017 Estimating and reporting detection limits for elements in homogeneous materials. Following the method outlined in ISO 19668:2017 the estimated minimum detection limits for common impurity elements in an α-Pu matrix using the survey spectrum shown in Figure 1 have been calculated and are detailed in Table 4 with the Pu4f spin orbit doublet as the reference intensity. The spectrum shown in Figure 1 has an O1s signal at approximately 10 % concentration, the standard deviation of the background intensity either side of this peak was used to calculate

the detection limit. The detection limits presented in Table 4 are relatively high as expected from the high Z material and density of the α-Pu matrix [51]. Furthermore, as highlighted earlier, hydrogen is a common impurity in plutonium metal and alloys as will be radiogenic helium in aged samples and it is currently not possible to detect these elements in solids using conventional laboratory based photoelectron spectrometers [52].

Table 4. Estimated minimum detection limits for selected elements in an α-Pu matrix

Element	**Transition**	**Detection limit (at. %)**
Carbon	1s	2.7
Nitrogen	1s	1.7
Oxygen	1s	1.2
Fluorine	1s	0.9
Iron	$2p_{3/2}$	0.6
Uranium	$U4f_{7/2}$	0.2

Conclusions

XPS data has been acquired of an α-Pu and δ-Pu(Ga) in the same spectrometer using identical conditions. The origin of the satellite peaks in the Pu4f peak shape in a sample of α-Pu and a δ-Pu(Ga) alloy have been further investigated. Both spectra showed the presence of small satellite feature at approximately 2.5 eV to higher binding which was lower intensity in the δ-Pu(Ga) alloy. The difference between the spectra afforded a similar shape and position acquired from Pu_2O_3. There was no difference in the Pu(NOV) X-ray induced Auger spectra of these two materials. The Pu4f spectra have been curve fit with an asymmetric and symmetric line shapes representative of metal and Pu_2O_3 respectively. The FWHM of the asymmetric peaks for the Pu4f spin orbit doublet of δ-Pu(Ga) were 0.1 eV greater than those in α-Pu. The pure element and alloy intensities were determined from extrapolation of multiple spectra acquired following in-situ oxidation experiments and the ratio of α-Pu / δ-Pu(Ga) intensity essentially identical to the expected theoretical atom density. The evidence presented here support the interpretation that the satellite feature occurs from Pu^{3+} impurities. However, we cannot discount the possibility of a poorly

screened satellite being present, albeit, of very low intensity and likely to be identical in both α-Pu and δ-Pu(Ga).

Experimental Relative Sensitivity Factors have been determined for the $Pu4p_{3/2}$, $Pu4d_{5/2}$, Pu4f and $Pu6p_{3/2}$ transitions and these have been applied to the quantification of the data presented here. The first example of quantification employed the different EAL of the $Pu4d_{5/2}$, Pu4f and $Pu6p_{3/2}$ transitions to show the Pu^{3+} species is 10-11 % at different depths investigated indicative of a bulk like impurity albeit relative to the technique being used. Quantification of the O1s and Pu4f intensities following in-situ oxidation in UHV afforded an average stoichiometry of $PuO_{1.6}$ in both the α-Pu and δ-Pu(Ga) substrates. The third example of XPS quantification was determination of the Ga content. This was particularly challenging as several of the Ga and Pu core level peaks overlap. It was found that this required curve fitting the $Pu6p_{3/2}$ region for both metal and oxide and the overlapping Ga3d peak shape. The RSFs reported here are applicable to spectrometers by the same manufacturer. Finally, the detection limits of some common impurity elements in plutonium metal and alloys have been calculated and are presented.

Acknowledgements

This work was performed under the auspices of the U.S. Department of Energy by Lawrence Livermore National Laboratory under contract DE-AC52-07NA27344. PR would like to thank D. Watson, Physical Electronics for useful discussions on data reduction and RSF determination.**ORCID**

Paul Roussel https://orcid.org/0000-0003-3061-4911

References

[1] J. M. Wills, O. Eriksson, Actinide ground state properties Theoretical predictions, Los Alamos Science, 26 (2000) 128.

[2] D. L. Clark, D. A. Geeson, R. J. Hanrahan (Eds.), Plutonium Handbook, 2nd ed., American Nuclear Society, La Grange Park, Illinois (2019).
[3] J. M. Haschke, T. H. Allen, L. A. Morales, Surface and corrosion chemistry of plutonium, Los Alamos Science, 26 (2000) 252.
[4] B. W. Veal, D. J. Lam, H. Diamond, H. R. Hoekstra, X-ray photoelectron spectroscopy study of the oxides of transuranium elements Np, Pu, Cm, Bk, and Cf, Phys. Rev. B 15 (1977) 2929.
[5] D. T. Larson, AES and XPS study of plutonium oxidation, J. Vac. Sci. Technol. 17 (1980) 55.
[6] R. Baptist, D. Courteix, J. Chayrouse, L. Heintz, J. Phys. F: Met. Phys., 12 (1982) 2103.
[7] D. T. Larson, J. M. Haschke, XPS-AES characterization of plutonium oxides and oxide carbide. The existence of plutonium monoxide, Inorg. Chem., 20 (1981) 1945.
[8] T. Gouder, L. Havela, Examples of quantification in XPS on 5f materials, Mikrochim. Acta, 138 (2002) 207.
[9] H. G. Garcia Flores, D. L. Pugmire, The growth and evolution of thin oxide films on d-plutonium surfaces, IOP Conf. Ser.:Mater. Sci. Eng. 9 (2010) 012038.
[10] H. G. Garcia Flores, P. Roussel, D. P. Moore, D. L. Pugmire, Characterization and stability of thin oxide films on plutonium surfaces, Surf. Sci., 605 (2011) 314.
[11] P. Morrall, P. Roussel, L. Jolly, A. Brevet, F. Delaunay, Determination of the clean 4f peak shape in XPS for plutonium metal, J. Nucl. Mater., 385 (2009) 15.
[12] C. D. Wagner, L. E. Davis, M. V. Zeller, J. A. Taylor, R. H. Raymond, L. H. Gale, Empirical atomic sensitivity factors for quantitative analysis by electron spectroscopy for chemical analysis, Surf. Interface Anal., 3 (1981) 211.
[13] J. H. Scofield, Hartree-Slater subshell photoionization cross-sections at 11254 and 1487 eV, J. Electron Spectros. Relat. Phenomena, 8 (1976) 129.
[14] N. Fairley, V. Fernandez, M. Richard-Plouet, C. Guillot-Deudon, J. Walton, E. Smith, D. Flahaut, M. Greiner, M. Biesinger, S. Tougaard, D. Morgan, J. Baltrusaitsis, Systematic and collaborative approach to problem solving using X-ray Photoelectron Spectroscopy, Appl. Surf. Sci. Adv., 5 (2021) 100112. DOI:10.1016/j.apsadv.2021.100112
[15] G. H. Major, T. G. Awal, D. I. Patel, D. Shah, T. Roychowdhury, A. J. Barlow, P. J. Pigram, M. Greiner, V. Fernandez, A. Herrera-Gomez, M. R. Linford, A discussion of approaches for fitting asymmetric signals in X-ray photoelectron spectroscopy (XPS), noting the importance of the Voigt-like peak shapes, Surf. Interface Anal., 53 (2021) 689.
[16] R. F, Reilman, A. Msezane, S. T. Manson, Relative intensities in photoelectron spectroscopy of atoms and molecules, J. Electron Spectros. Relat. Phenomena., 8 (1976) 389.
[17] M. P. Seah, Simple universal curve for the energy-dependant electron attenuation length for all materials, Surf. Interface Anal. 44 (2012) 1353. DOI:10.1002/sia.5033.
[18] P. Roussel, Inverse photoemission measurements of plutonium metal and oxides, J. Electron Spectros. Relat. Phenomena., 246 (2021) 147030.
[19] G. van der Laan, M. Taguchi, Valence fluctuations in thin films and a and d phases of Pu metal determined by 4f core-level photoemission calculations, Phys. Rev. B 82 (2010) 045114.
[20] W. F. Egelhoff, Core-level binding-energy shifts at surfaces and in solids, Surf. Sci. Rep., 6 (1987) 253.

[21] G. van der Laan, K. T. Moore, J. G. Tobin, B. W. Chung, M. A. Wall, A. J. Schwartz, Applicability of the spin-orbit sum rule for the actinide 5f states, Phys. Rev. Lett., 93 (2004) 097401.
[22] S. P Kowalczyk, L. Ley, F. R. McFeely, D. A. Shirley, Multiplet splitting of the manganese 2p and 3p levels in MnF2 single crystals, Phys. Rev. B, 11 (1975) 1721.
[23] J. C. Fuggle, M. Campagna, Z. Zolnierek, R. Lasser, A. Platau, Observation of a relationship between core-level line shapes in photoelectron spectroscopy and the localization of screening orbitals, Phys. Rev. Lett., 45 (1980) 1597.
[24] J. R. Naegele, L. Manes, J. C. Spirlet, W. Muller, Localization of 5f electrons in americium: A photoemission study, Phys. Rev. Lett., 52 (1984) 1834.
[25] L. E. Cox, X-ray photoemission study of δ-Pu stabilized by 1 wt. % Ga: Electronic structure and sputter-induced surface phase transformation, Phys. Rev. B 37 (1988) 8480.
[26] L. E. Cox, O. Eriksson, B. R. Cooper, Variable-takeoff-angle x-ray-photoelectron-spectroscopy evidence for an electronically modified surface in α-Pu, Phys. Rev. B 46 (1992) 13571.
[27] J. Terry, R. K. Schulze, J. D. Farr, T. Zocco, K. Heinzelman, E. Rotenberg, D. K. Shuh, G. van der Laan, D. A. Arena, J. G. Tobin, 5f resonant photoemission from plutonium, Surf. Sci. 499 (2002) L141.
[28] P. Roussel, A. J. Bishop, A. F. Carley, Surf. Sci. 714 (2021) 121914.
[29] T. Gouder, L. Havela, A. B. Shick, F. huber, F. Wastin, J. Rebizant, Variability of 5f states in plutonium carbides, J. Phys.:Condens. Matter 19 (2007) 476201.
[30] D. Courteix, J. Chayrouse, L. Heintz, XPS study of plutonium oxides, R. Baptist, Solid State Commun. 39 (1981) 209.
[31] L. Havela, F. Wastin, J. Rebizant, T. Gouder, Photoelectron spectroscopy study of PuN, Phys. Rev. B 68 (2003) 085101.
[32] A. J. Nelson, W. K. Grant, J. A. Stanford, W. J. Siekhaus, P. G. Allen, W. McLean, X-ray excited Auger transitions of Pu compounds, J. Vac. Sci. Technol. A 33 (2015) 031401.
[33] P. Roussel, D. S. Shaw, D. A. Geeson, Initial studies of plutonium corrosion, J. Nucl. Sci. Technol., 39:sup3 (2002) 78. DOI: 10.1080/00223131.2002.10875412.
[34] A. J. Nelson, P. Roussel, Low temperature oxidation of plutonium, J. Vac. Sci. Tech. A 31 (2013) 031406.
[35] C. R. Brundle, B. V. Crist, X-ray photoelectron spectroscopy: a perspective on quantification accuracy for compositional analysis of homogeneous materials, J. Vac. Sci. Technol. A., 38 (2020) 041001.
[36] J. -N. Chazalviel, M. Campagna, G. K. Wertheim, P. H. Schmidt, Y. Baer, Electronic structure and 4f-hole lifetime in rare-earth borides, Phys. Rev. Lett., 37 (1976) 919
[37] G. G. Kleiman, Electronic structure information of metals and alloys from auger and photoemission, J. Mol. Catal. A Chem., 228 (2005) 137.
[38] D. T. Larson, K. M. Motyl, Detection of plutonium hydride using X-ray photoelectron spectroscopy, J. Electron Spectros. Relat. Phenomena., 50 (1990) 67.
[39] A. G. Shard, Practical guides for X-ray photoelectron spectroscopy: Quantitative XPS, J. Vac. Sci. Technol. A 38 (2020) 041201; DOI:10.1116/1.5141395.

[40] Theoretical Pu atom density were calculated using equations A.11 and A.12 in ISO 18118 "Guide to the use of experimentally determined relative sensitivity factors for the quantitative analysis of homogeneous materials"
[41] T. Gouder, F. Wastin, J. Rebizant, L. Havela, 5f-electron localization in PuSe and PuSb, Phys. Rev. Lett., 84 (2000) 3378.
[42] J. Ghijsen, Photoemission study (XPS, UPS) of $PuFe_2$, J. Electron Spectros. Relat. Phenomena, 35 (1985) 19.
[43] C. P. Opeil, R. K. Schulze, M. E. Manley, J. C. Lashley, W. L. Hults, R. J. Hanrahan, J. L. Smith, B. Mihaila, K. B. Blagoev, R. C. Albers, P. B. Littlewood, Phys. Rev. B 73 (2006) 165109.
[44] G. H. Major, N. Fairley, P. A. Sherwood, M. R. Linford, J. Terry, V. Fernandez, K. Artyushkova, Practical guide for curve fitting in x-ray photoelectron spectroscopy, J. Vac. Sci. technol. A 38 (2020) 061203.
[45] J. F. Moulder, W. F. Stickle, P. E. Sobol, K. D. Bomben, Handbook of X-ray photoelectron spectroscopy: A reference book of standard spectra for identification and interpretation of XPS data, Physical Electronics, Eden-Prairie, MN (1992).
[46] J. C. Vickerman, D. Briggs (Eds.), ToF-SIMS Surface analysis by mass spectrometry, IM Publications (2001).
[47] E. R. Gardner, T. L. Markin. R. S. Street, The plutonium-oxygen phase diagram, J. Inorg. Nucl. Chem., 27 (1965) 541.
[48] H. G. Garcia-Flores, Characteristics and stability of oxide films on plutonium surfaces, Ph.D. Thesis, University of Nebraska – Lincoln, 2010.
[49] P. Cakir, R. Eloirdi, F. Huber, R. J. M. Konings, T. Gouder, An XPS and UPS study of the electronic structure of ThO_x ($x \leq 2$) thin films, J. Phys. Chem. C 118 (2014) 24497. DOI: 10.1021/jp506750p.
[50] F. Gerkin, A. S. Flodstrom, J. Barth, L. I. Johansson, C. Kunz, Surface core level shifts of the lanthanide metals Ce^{58}-Lu^{71}:A comprehensive experimental study, Phys. Scr., 32 (1985) 43.
[51] A. G. Shard, Detection limit in XPS for more than 6000 binary systems using Al and Mg Kα X-rays, Surf. Interface Anal., 46 (2014) 175.
[52] J-Q. Zhong, M. Wang, W. H. Hoffmann, M. A. van Spronsen, D. Lu, J. A. Boscoboinik, Appl. Phys. Lett., 112 (2018) 091602.

Tables

Figure Captions

Supporting information

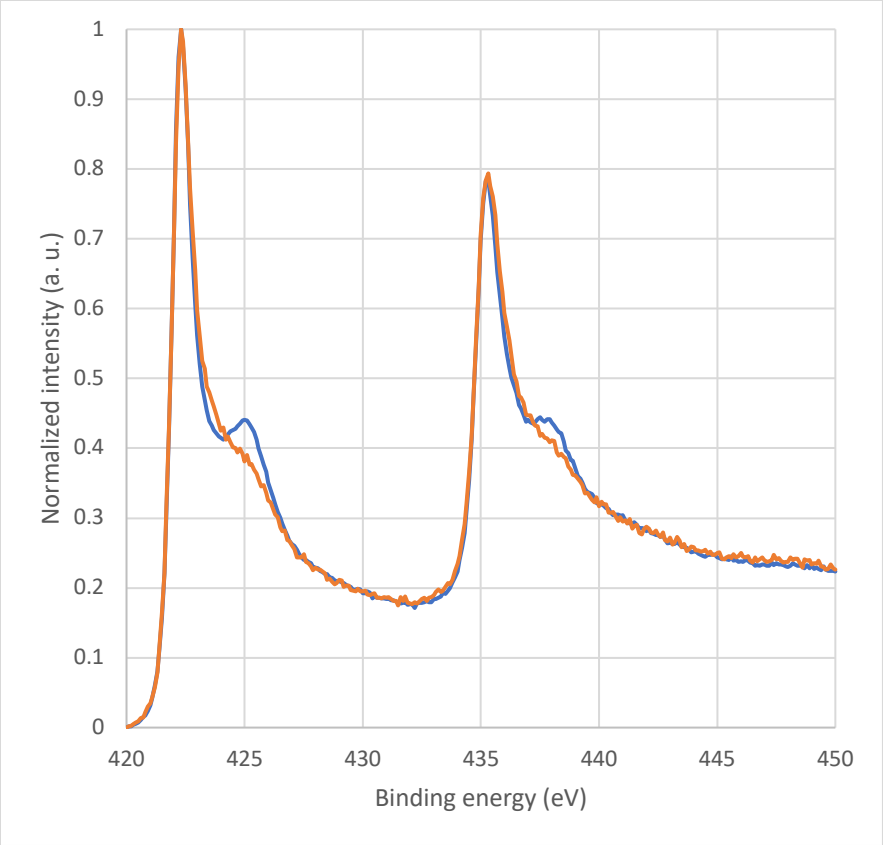

The Pu4f spectra from Figure 2 of α-Pu (blue) overlaid with δ-Pu(Ga) (red).

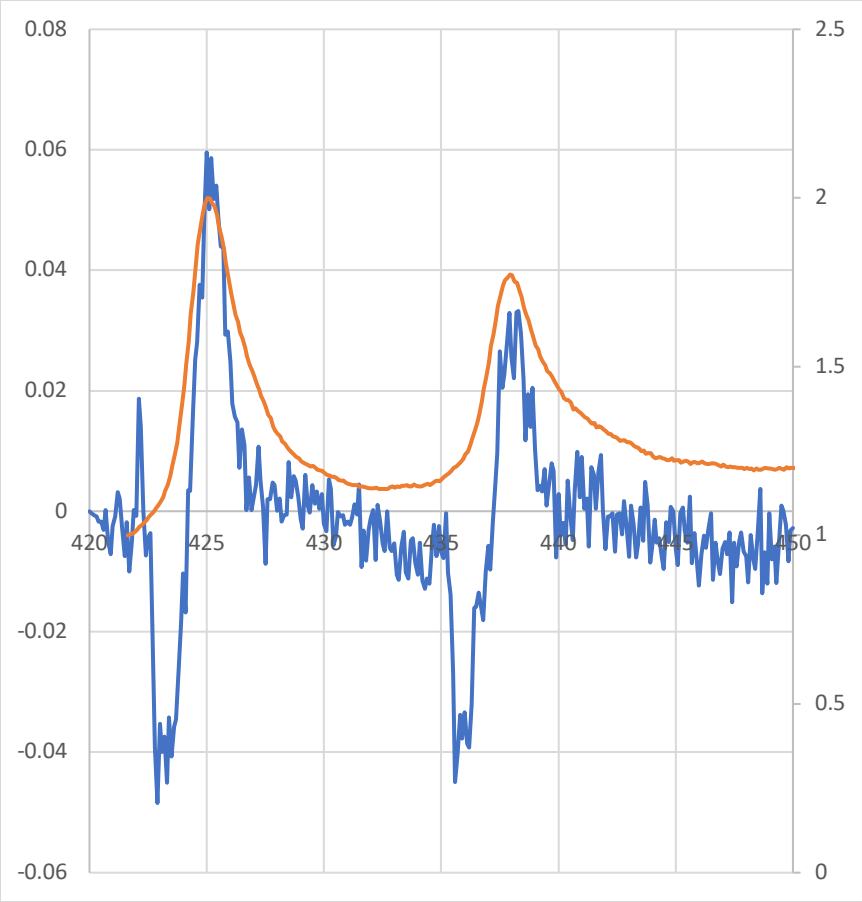

The difference spectrum (blue) obtained by subtracting the δ-Pu(Ga) Pu4f shown above from the α-Pu spectrum. The Pu4f spectrum of Pu_2O_3 (red) is from Figure 2

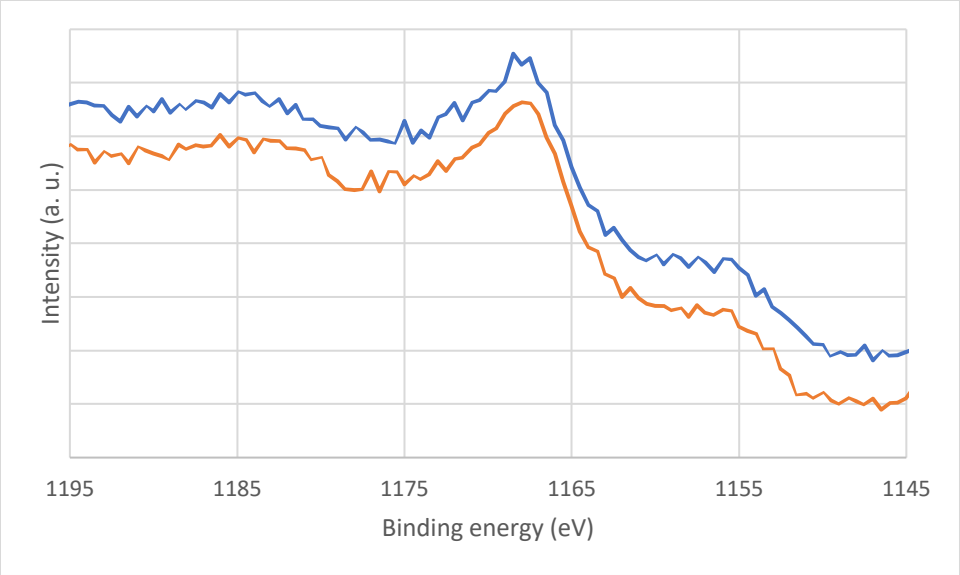

Pu(NOV) X-ray induced Auger peak for α-Pu (blue) and δ-Pu(Ga) (orange). No difference was observed in the as acquired spectra shown above or the first derivative.

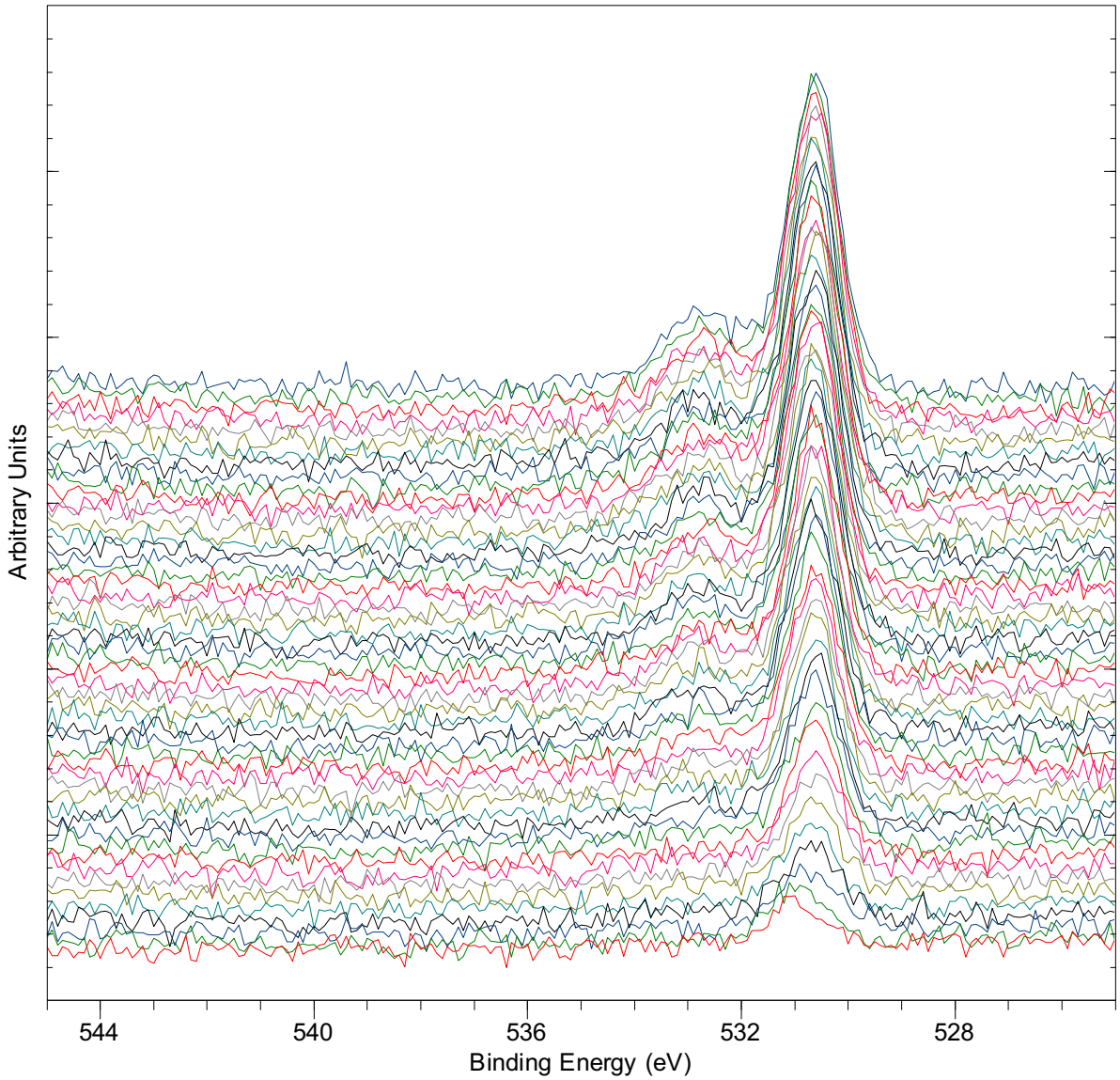

O1s spectra acquired following the in-situ oxidation of the α-Pu sample in UHV (time increasing from bottom to top)

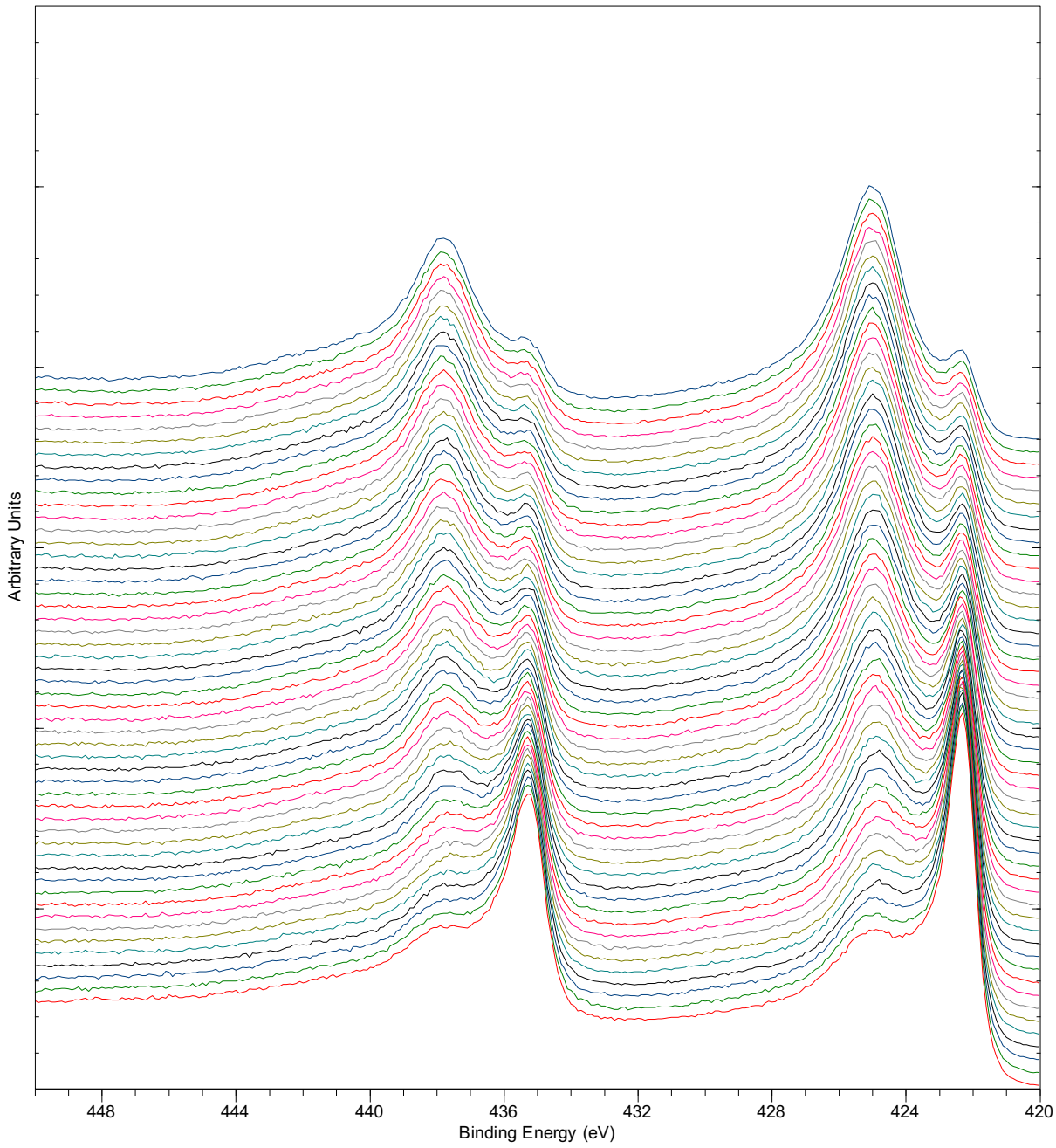

Pu4f spectra acquired following the in-situ oxidation of the α-Pu sample in UHV (time increasing from bottom to top)